# Optical imaging in an Alzheimer's mouse model reveals amyloid-*β*-dependent vascular impairment

Alexander J. Lin
Gangjun Liu
Nicholas A. Castello
James J. Yeh
Rombod Rahimian
Grace Lee
Victoria Tsay
Anthony J. Durkin
Bernard Choi
Frank M. LaFerla
Zhongping Chen
Kim N. Green
Bruce J. Tromberg

# Optical imaging in an Alzheimer's mouse model reveals amyloid-$\beta$-dependent vascular impairment

Alexander J. Lin,[a,c] Gangjun Liu,[a] Nicholas A. Castello,[b,d] James J. Yeh,[a] Rombod Rahimian,[a] Grace Lee,[a] Victoria Tsay,[a] Anthony J. Durkin,[a] Bernard Choi,[a,c] Frank M. LaFerla,[b,d] Zhongping Chen,[a,c] Kim N. Green,[b,d] and Bruce J. Tromberg[a,c,*]

[a]Beckman Laser Institute and Medical Clinic, Laser Microbeam and Medical Program, 1002 Health Sciences Road, Irvine, California 92612
[b]University of California Irvine, Institute for Memory Impairments and Neurological Disorders, 2642 Biological Sciences III Irvine, California 92697-4545
[c]University of California Irvine, Department of Biomedical Engineering, 3120 Natural Sciences II, Irvine, California 92697-2715
[d]University of California Irvine, Department of Neurobiology and Behavior, 2205 McGaugh Hall, Irvine, California 92697-4550

**Abstract.** Alzheimer's disease (AD) and cerebrovascular disease are often comorbid conditions, but the relationship between amyloid-$\beta$ and *in vivo* vascular pathophysiology is poorly understood. We utilized a multimodal, multiscale optical imaging approach, including spatial frequency domain imaging, Doppler optical coherence tomography, and confocal microscopy, to quantify AD-dependent changes in a triple transgenic mouse model (3xTg-AD) and age-matched controls. From three months of age (naïve) to 20 months (severe AD), the brain tissue concentration of total and oxy-hemoglobin (Total Hb, $ctO_2Hb$) decreased 50 and 70%, respectively, in 3xTg-AD mice. Compared to age-matched controls, significant differences in brain hemoglobin concentrations occurred as early as eight months (Total Hb: $126 \pm 5$ $\mu$M versus $108 \pm 4$ $\mu$M; $ctO_2Hb$: $86 \pm 5$ $\mu$M versus $70 \pm 3$ $\mu$M; for control and AD, respectively). These changes were linked to a 29% vascular volume fraction decrease and 35% vessel density reduction in the 20-month-old 3xTg-AD versus age-matched controls. Vascular reduction coincided with increased brain concentration of amyloid-$\beta$ protein, vascular endothelial growth factor (VEGF), and endothelial nitric oxide synthase (eNOS) at eight and 20 months compared to the three-month baseline. Our results suggest that amyloid-$\beta$ blocks the normally reparative effects of upregulated VEGF and eNOS, and may accelerate *in vivo* vascular pathophysiology in AD. © The Authors. Published by SPIE under a Creative Commons Attribution 3.0 Unported License. Distribution or reproduction of this work in whole or in part requires full attribution of the original publication, including its DOI. [DOI: 10.1117/1.NPh.1.1.011005]

Keywords: spatial frequency domain imaging; Doppler optical coherence tomography; vascular reactivity; hypercapnia; microvascular perfusion; diffuse optical spectroscopy; scattering; absorption; neuroimaging.

Paper 14019SSR received Feb. 28, 2014; revised manuscript received Apr. 21, 2014; accepted for publication Apr. 28, 2014; published online May 28, 2014.

## 1 Introduction

Cerebrovascular pathology is often a comorbidity of Alzheimer's disease (AD).[1] In patients, 60 to 90% of AD cases are associated with ischemic vascular disease and 90% of cases show amyloid-$\beta$ deposition in the vessels.[2] Blood vessels become less pliable early in the process of AD, and this lack of vessel reactivity has been detected with transcranial Doppler,[3–5] fMRI,[6,7] PET,[8] and SPECT (Ref. 9) techniques. The reduced vascular reactivity is also seen in mouse models genetically modified to overexpress amyloid-$\beta$ pathology,[10] and these mice are rescued from pathology and memory impairment when treated with anti-hypertensive drugs[11] or Viagra (regulates nitric oxide pathway).[12] A proposed hypothesis of AD pathogenesis is that reduced oxygen delivery to the brain leads to hypoxic stress in neurons, causing further amyloid-$\beta$ production[13,14] and vessel damage.[1] However, it is unknown (1) when the brain becomes hypoxic, (2) how hypoxic the brain becomes, and (3) the role of vessel constriction versus vessel loss in AD-related hypoxia.

Diffuse optical imaging (DOI)[15] quantitatively measures the tissue concentration of oxy- and deoxy-hemoglobin, making it well-suited for studies of brain hemodynamics. We recently described intrinsic optical and hemodynamic contrast between 20-month-old triple-transgenic APP/tau/presenilin 1 (3xTg-AD) mice and age-matched controls *in vivo* using spatial frequency domain imaging (SFDI), a noncontact, camera-based DOI technique.[16] SFDI employs a model of light transport to solve for tissue absorption ($\mu_a$) and reduced scattering ($\mu_s'$) coefficients on a pixel-by-pixel basis.[17] Oxy- and deoxy-hemoglobin concentrations were derived from the $\mu_a$ spectra (650 to 970 nm) using the Beer-Lambert law. Compared to age-matched controls, the 3xTg-AD mice had 16 and 21% lower total and oxy-hemoglobin concentrations. A dynamic hyperoxia inhalation challenge also revealed half the functional response found in controls.

In this study, we utilized SFDI to characterize how and when this hypoxic state arises in the 3xTg-AD mouse model compared to age-matched controls. Doppler optical coherence tomography (dOCT) was also used to detect cortical vascular volume *in vivo* in some 20-month-old animals. After imaging, the mice were sacrificed and vessel density was counted using confocal microscopy, and brain protein levels of amyloid-$\beta$, endothelial nitric oxide synthase (eNOS), neuronal nitric oxide synthase (nNOS), and vascular endothelial growth factor (VEGF) were measured. We assumed the toxic effects of amyloid-$\beta$ on the brain vasculature are global, allowing comparison between the various sampling depths and volumes of the

multiple imaging modalities used. This multimodal optical imaging approach allowed us to show that brain hypoxia occurs as early as eight months in the 3xTg-AD brain; vessel constriction and vessel loss both contribute to reduced blood perfusion, and the normal vasodilatory and angiogenic effects of eNOS and VEGF, respectively, may be blocked by amyloid-$\beta$.

## 2 Materials and Methods

### 2.1 Animal Model

All mice used were bred and obtained from the LaFerla laboratory at University of California, Irvine. 3xTg-AD mice were studied at three months ($n = 9$), eight months ($n = 6$), and 20 months of age ($n = 5$) to coincide with naïve, moderate, and advanced plaque and tangle pathology, respectively. Age-matched C57 BL/6-129svj mice (three months: $n = 6$; eight months: $n = 6$; 20 months: $n = 9$) were used to control for changes due to normal aging. All procedures were performed in accordance with the regulations of the Institutional Animal Care and Use Committee of the University of California, Irvine (protocol no. 2010-2934).

Imaging windows were created under gas mask isoflurane anesthesia (2% maintenance in 21% oxygen balanced by nitrogen) by removing the skin from bregma anteriorly to lambda posteriorly and bilaterally to the temporalis muscle attachments. The mouse skull, 200- to 500-$\mu$m thick, was left intact to reduce trauma artifact from removing or thinning it. This approach has been used widely in intrinsic signal imaging of mouse brain.[18] During the initial surgery and for the imaging session, the mouse was kept at 37°C by a thermister-controlled heating pad (CWE Inc., Ardmore, Pennsylvania). The mouse's head was secured in a stereotactic frame (Stoelting Co, Wood Dale, Illinois) to prevent motion and a thin layer of mineral oil was applied onto the cranium to reduce skull drying.[19,20] Following surgery, isoflurane was turned down to 1% maintenance. Excess gases were scavenged via a *f/air* adsorber unit (A.M. Bickford Inc., Wales Center, New York) and gas flow was maintained at 1 L/min.

### 2.2 Steady-State Measurement and Hypercapnia Challenge

An initial 17-wavelength (650 to 970 nm, every 20 nm) baseline measurement was acquired in triplicate, lasting for ~2 min with the mouse breathing 21% $O_2$ (normoxia). Immediately following the 17-wavelength scan, in 20-month-old mice, baseline and dynamic measurements were recorded during an eight-min vasodilation challenge using only 670- and 850-nm light to achieve a time resolution of ~5 s/measurement while still containing hemoglobin chromophore information. Normoxia was used to measure the baseline optical properties again for three min followed by hypercapnia (5% $CO_2$, 95% normoxia air) as an experimental perturbation for five min.

### 2.3 SFDI Instrument and Analysis

A schematic of the experimental arrangement is illustrated in Fig. 1. A complete description of SFDI instrumentation and data analysis has been previously presented in detail.[16,17,21] Briefly, broadband near-infrared light was projected onto the mouse cranium in sinusoidal patterns at two spatial frequencies (0 and 0.125 mm$^{-1}$) and phase-shifted 120 deg apart (six projections total), and the remitted reflectance was captured at 17
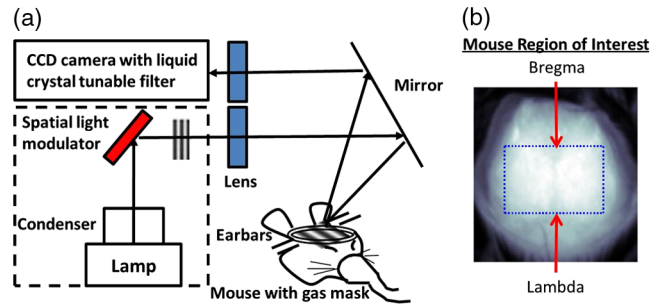


**Fig. 1** Schematic of spatial frequency domain imaging (SFDI) setup (a) and region of interest (ROI) (b).

wavelengths from 650 to 970 nm by a Nuance Multispectral Imaging System (CRI Inc., Woburn, Massachusetts) with a liquid-crystal tunable filter. The phase-shifted images (e.g., $I_1$, $I_2$, $I_3$) were demodulated [Eq. (1)] and calibrated to a mouse-shaped silicone phantom of known optical properties to correct for any system response, such as light inhomogeneity or lens aberrations. A known Monte Carlo forward model[21] was then used to generate a look-up table to solve for $\mu_a$ and $\mu_s'$ pixel-by-pixel.

$$M_{AC} = \frac{\sqrt{2}}{3}\sqrt{[(I_1 - I_2)^2 + (I_2 - I_3)^2 + (I_3 - I_1)^2]}. \quad (1)$$

Quantitative tissue concentration values of oxy-hemoglobin (ct$O_2$Hb), deoxy-hemoglobin (ctHHb), total hemoglobin (THb = ct$O_2$Hb + ctHHb), and tissue oxygen saturation ($S_tO_2 = 100 * ctO_2Hb/Total Hb$) were calculated from the absorption spectrum according to the Beer-Lambert law using a least squares linear fit. For further analysis, a region of interest (ROI) was selected between the suture junctions, bregma and lambda, and bilaterally to the temporalis muscle attachments (Fig. 1). The average of pixel intensities in the ROI for each mouse was calculated. The within-group standard deviation (i.e., 3xTg-AD versus control) was calculated using the average ROI pixel values for each mouse in the group. All averages, standard error bars, and $p$ values shown were calculated from mean ROI and SD values between animals in each group. A two-tailed student's $t$-test analysis was used to determine significance between Alzheimer's and control mice. All image processing and analyses were done with MATLAB® software (Mathworks, Natick, Massachusetts).

### 2.4 Doppler Optical Coherence Tomography

After SFDI, some 20-month-old mice (three Ctrl versus three 3xTg-AD) were imaged with dOCT *in vivo* while breathing 21% $O_2$. A fiber-based swept source OCT system with a central wavelength of 1310 nm, an A-line rate of 50,000 Hz, and sensitivity of 108 dB was used in the experiment. The system has a depth resolution of 9.3 $\mu$m in air and a lateral resolution of ~9 $\mu$m. For *in vivo* mouse brain vasculature mapping, a three-dimensional (3-D) OCT data volume containing 4096 frames with 1024 A-lines per frame was obtained for each sample and the processed 3-D OCT volume covered an area of ~2 mm × 2 mm × 3 mm. A recently developed intensity-based Doppler variance method was used to reconstruct the cortical vessel network.[22] In each A-line, the OCT system provided 512 pixels over a depth of 4.3 mm in air (~3 mm in tissue). However, because of scattering from the overlying skull and

the shadowing artifact from the high density of blood vessels in mouse brain, dOCT analysis was limited to the superficial vessels of the brain.

The en-face dOCT images obtained were analyzed to calculate vessel volume fraction. Vessel volume fraction was calculated from the most superficial (color-labeled white) layer (180 $\mu$m thickness). For each mouse, 30 en-face images imported into MATLAB® were intensity-thresholded using the MATLAB® function *greythresh*, which applies Otsu's method, and a $7 \times 7$ pixel median filter was applied. Vessel volume fraction was calculated as the number of pixels with vessels throughout the tissue volume divided by the total number of pixels in the tissue volume. Mean apparent hematocrit was calculated from Eq. (2).

$$\text{Mean Hematocrit} = \frac{\text{THb}\left(\frac{\mu\text{mol}}{1000\,\text{ml}}\right)}{\text{Volume Fraction}} * \frac{0.0645\,g\,\text{hemoglobin}}{\mu\text{mol}}$$
$$* \frac{1\,\text{ml}\,\text{red blood cells}}{0.3\,g\,\text{hemoglobin}}, \qquad (2)$$

where THb is the mean ROI total hemoglobin value determined from SFDI measurements and hemoglobin weight per 1 ml packed red blood cells is derived from young C57 BL/6J mice.[23]

For 3-, 8-, and 20-month-old mice, we saved the overlying skull and a single OCT B-scan frame was obtained for each sample *ex vivo*. Using ImageJ software,[24] the distance (pixel number) between the upper and lower skull boundary was found manually at three points and multiplied by the pixel resolution

(6 $\mu$m/px) to determine the average thickness of each mouse skull.

### 2.5 Histology

In 3- and 20-month animals, 150 $\mu$l of 10 mg/ml Texas Red lysine-fixable dextran dye (Invitrogen, Grand Island, New York) was administered via cardiac injection prior to sacrificing the animals. The right hemispheres of the brains were preserved in 10% formalin and subsequently flash frozen and sliced in horizontal sections to correlate to the top-down imaging of SFDI. Citrate-treated 40-$\mu$m slices were incubated overnight at 4°C with eNOS primary antibodies (Abcam, Cambridge, Massachusetts) diluted 1:400 and/or amyloid-$\beta$ 6e10 primary antibodies (Millipore, Bellerica, Massachusetts) diluted 1:500 and the appropriate secondary fluorescent antibodies. Cortical slices (40 $\mu$m) ~300 $\mu$m down from the dorsal surface of the brain were selected and imaged with confocal microscopy for the vessel-labeling dextran and eNOS. Vessel density analysis was done on either the dextran (3- and 20-month animals) or eNOS images (8-month animals) with a semiautomated code written in MATLAB®,[25] with user-defined thresholds for intensity and object size of the vessels. Mean vessel density was calculated as the total length of the vessels in the image divided by the area of the image. Three to six animals were used in each group for statistical analyses.

### 2.6 Western Blots

The left hemisphere of each brain was flash frozen and soluble homogenates of the forebrain were run on a polyacrylamide gel
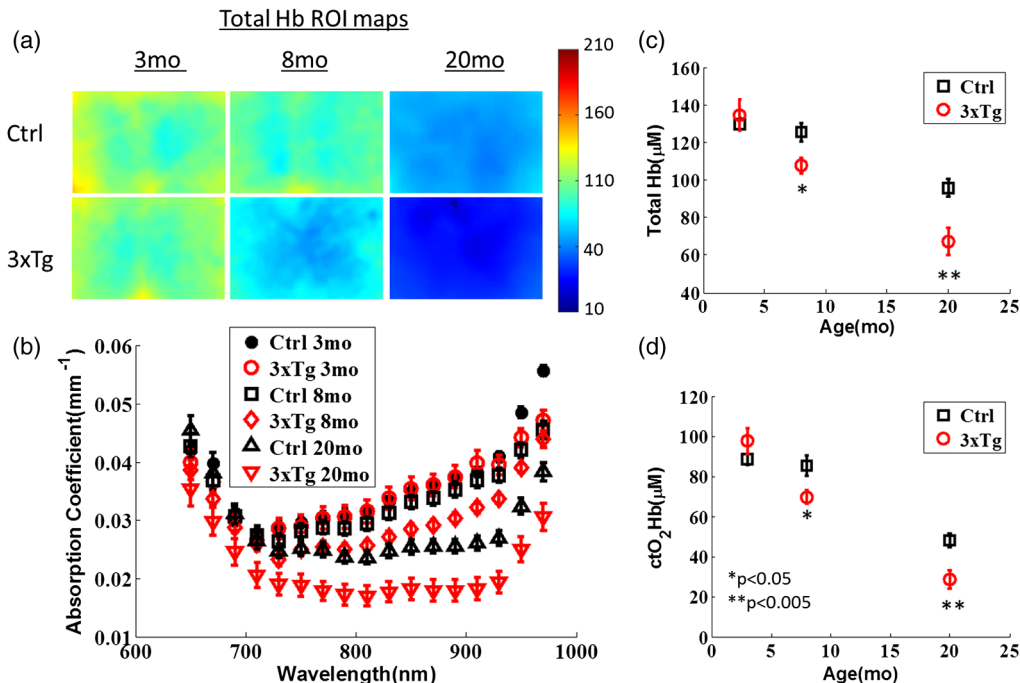


**Fig. 2** (a) ROI images of total hemoglobin concentration (Total Hb) for control (Ctrl) and AD (3xTg) mice determined from *in vivo* SFDI measurements. (b) Average ROI absorption spectra for 3, 8, and 20 month-old 3xTg-AD (red) and age-matched controls (black) show decreased absorption with age and disease. (c) Average ROI total hemoglobin concentration versus age shows significant decrease in 3xTg-AD mice by eight months of age. (d) Average ROI oxy-hemoglobin (ctO$_2$Hb) concentration versus age shows significant decrease in 3xTg-AD mice by eight months of age. All error bars are standard error between animals in each group.

**Table 1** Baseline mean ROI concentrations of tissue oxy-hemoglobin (ctO$_2$Hb), deoxy-hemoglobin (ctHHb), total hemoglobin (Total Hb), and hemoglobin oxygen saturation (S$_t$O$_2$) for each group. *$p < 0.05$, **$p < 0.01$.

|  | ctO$_2$Hb ($\mu$m) | ctHHb ($\mu$m) | Total Hb ($\mu$m) | S$_t$O$_2$ (%) |
|---|---|---|---|---|
| 3 m Ctrl | 117 ± 3 | 52 ± 2 | 168 ± 4 | 69 ± 1 |
| 3 m 3xTg | 126 ± 7 | 47 ± 2 | 173 ± 8 | 73 ± 1* |
| 8 m Ctrl | 114 ± 5 | 51 ± 3 | 164 ± 5 | 69 ± 2 |
| 8 m 3xTg | 98 ± 3* | 48 ± 1 | 146 ± 4* | 67 ± 1 |
| 20 m Ctrl | 77 ± 3 | 58 ± 3 | 135 ± 5 | 57 ± 1 |
| 20 m 3xTg | 58 ± 5** | 49 ± 3 | 106 ± 7** | 54 ± 1 |

and probed with antibodies for amyloid-$\beta$ 6e10 (Signet, Dedham, Massachusetts), eNOS (Abcam), nNOS (Abcam), VEGF (Millipore, Temecula, California), and glyceraldehyde 3-phosphate dehydrogenase (GAPDH) (Santa Cruz Biotechnologies, Santa Cruz, California). Protein band intensities were analyzed with ImageJ software and normalized to the GAPDH band intensity. Relative comparisons were done between groups from a 26-well gel with four to five mice in each group.

## 3 Results

### 3.1 Baseline SFDI Brain Measurements

Optical property map ($\mu_a$ and $\mu_s'$) images of the brain were determined at 21% O$_2$ from 650 to 970 nm at 17 wavelengths spaced every 20 nm. Absorption contrast from 730 to 970 nm decreased significantly ($p < 0.05$) from 3 to 20 months of age in both Alzheimer's and control mice [Fig. 2(b)]. Significant absorption differences were also found between 8-month-old 3xTg-AD and control mice from 790 to 930 nm and between 20-month-old cohorts at all 17 wavelengths measured from 650 to 970 nm.

We found that normal aging from 3 to 20 months of age caused a 26, 46, and 26% decrease in Total Hb, ctO$_2$Hb, and tissue hemoglobin oxygen saturation (S$_t$O$_2$), respectively.
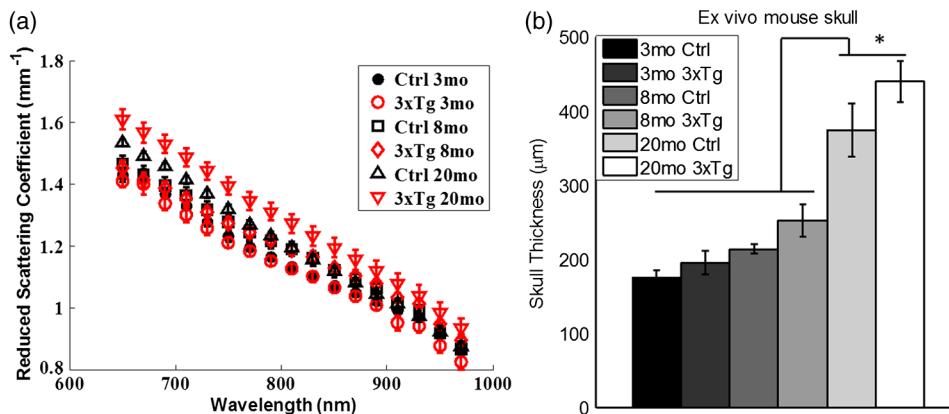
Similarly, aging in the 3xTg-AD model caused a 50, 70, and 42% decrease in Total Hb, ctO$_2$Hb, and S$_t$O$_2$, respectively. Total hemoglobin maps [Fig. 2(a)] illustrate the progression of perfusion decrease in normal and 3xTg-AD aging, and ROI averages for total hemoglobin [Fig. 2(c)] and ctO$_2$Hb [Fig. 2(d)] show that significant differences occur at 8 and 20 months of age. Table 1 has the calculated baseline ROI averages of hemoglobin concentrations at each age and condition group.
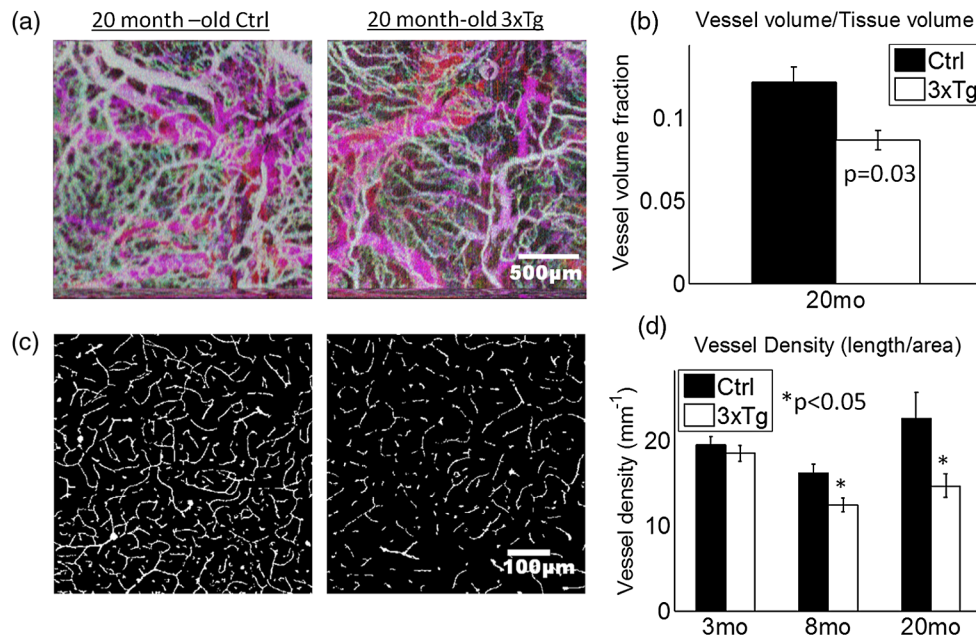
Reduced scattering values from 650 to 830 nm rose significantly ($p < 0.05$) in normal aging from 3 months to 20 months of age [Fig. 3(a)]. The same aging in 3xTg-AD mice caused significant scattering rises in all 17 wavelengths from 650 to 970 nm. Scattering was also significantly higher in the 20-month 3xTg-AD mice compared to age-matched controls from 650 to 890 nm. Skull thicknesses as measured by OCT ranged from 175 to 474 $\mu$m and increased significantly from the three- and eight-month time points to the 20-month time point [Fig. 3(b)].

### 3.2 In Vivo Doppler OCT

To better determine vascular tone *in vivo*, we looked at dOCT images of 20-month 3xTg-AD and control mice. As can be seen in Fig. 4, superficial cortical vessels (white) are more dilated in the controls and thinner in the 3xTg-AD mice. Analysis of the superficial vessel volumes reveal a 29% decrease ($p = 0.03$) in vessel volume in 3xTg-AD mice compared to controls [Fig. 4(b)]. Using Eq. (2) and the dOCT and SFDI data, the calculated apparent hematocrit was $0.16 \pm 0.02$ for 20-month controls and $0.17 \pm 0.03$ for 20-month 3xTg-AD mice ($p = 0.8$). Error reported is standard error.

### 3.3 Vessel Density Analysis

Immunohistochemistry revealed capillary staining in both control and 3xTg-AD mice at all three ages in cerebral blood vessels (Fig. 5). While eNOS capillary staining could also be seen in 3- and 20-month mice, the signal-to-noise was much better with the injected dextran dye. Amyloid-$\beta$ plaques could be seen in the cortex of 20-month-old 3xTg-AD mice. Images of the capillary staining were filtered into binary images [Fig. 4(c)] and skeletonized. When vessel density was analyzed, no significant



**Fig. 3** (a) Spectral dependence of reduced scattering parameter, shown for 3, 8, and 20 month-old 3xTg-AD (red) and age-matched controls (black). (b) Optical coherence tomography (OCT) analysis of skull thickness shows significant increase of skull thickness from 3 and 8 months of age to 20 months of age ($p < 0.05$). All error bars are standard error between animals in each group.

**Fig. 4** (a) Doppler OCT images of cortical vessels in 20-month control and 3xTg-AD mice. Superficial vessels (∼200 μm) are in white and deeper vessels are in pink. Scale bar is 500 μm. (b) Quantification of the superficial vessel (white) area in each group. (c) Computer-processed images of vessel density differences between 20-month control and 3xTg-AD mice derived from immunohistochemistry analysis. Scale bar is 100 μm. (d) Quantification of the cortical vessel density in each group.

difference was found between control and 3xTg-AD mice at the three-month time point [Fig. 4(d)]. Compared to the three-month time point, vessel density decreased 33% in the 3xTg-AD mice at the eight-month time point ($p < 0.05$) and 21% at 20 months. Vessel density was 23% lower ($p < 0.05$) and 35% lower ($p < 0.05$) in the 8- and 20-month 3xTg-AD mice compared to age-matched controls, respectively.

### 3.4 Western Blots

We confirmed with protein analysis that amyloid-β is elevated in the 8- and 20-month 3xTg-AD mice [Fig. 6(a)]. Both eNOS and VEGF were upregulated significantly by eight months, and eNOS continued to be significantly raised at 20 months for both 3xTg-AD and age-matched controls [Fig. 6(b)]. Protein expression of nNOS remained constant at all ages for both 3xTg-AD and controls.

### 3.5 Hypercapnia Vasodilation Challenge

To visualize the brain reactivity to hypercapnia, continuous measurements of 670/850 nm $\mu_a$ values were fit for concentrations of $ctO_2Hb$ and ctHHb and three-min baselines at normoxia and hypercapnia were averaged. In this vasodilation challenge, a rise in $ctO_2Hb$, Total Hb, and $S_tO_2$ along with a dip in ctHHb were expected and seen in the control mice [Fig. 6(c)]. Interestingly,
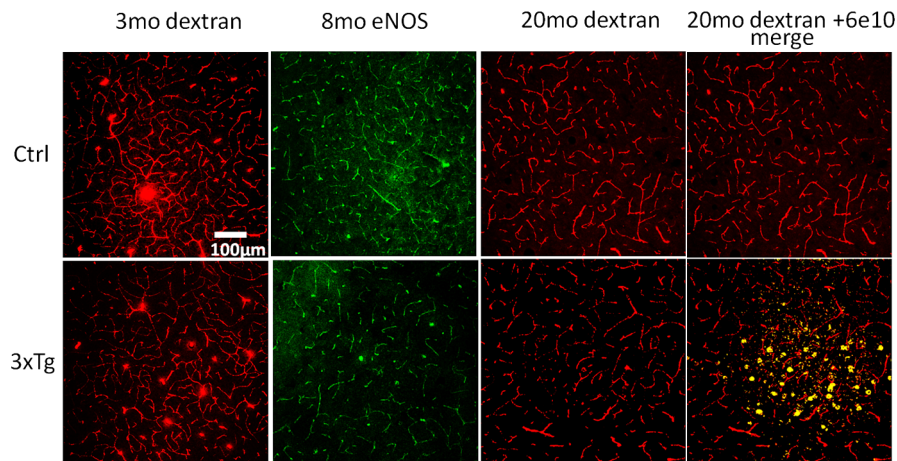


**Fig. 5** Images of capillary staining at 3, 8, and 20 months in controls and 3xTg-AD mice. Texas red dextran perfused into the vessels was used to label the 3- and 20-month mice and endothelial nitric-oxide synthase labeling was used to label the 8-month-old mice. Amyloid-β plaques (6e10 labeling) can be seen in the 20-month 3xTg-AD mice.
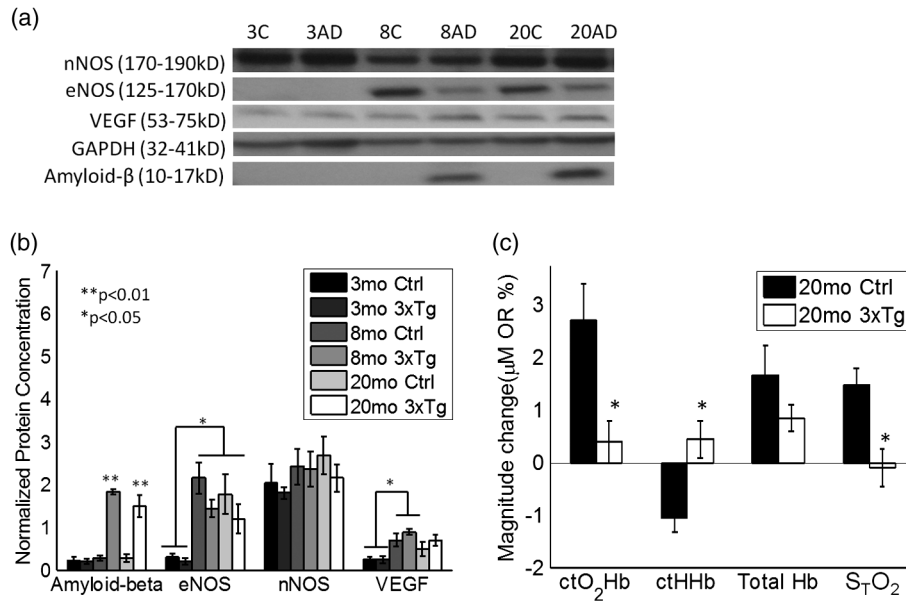
**Fig. 6** (a) Representative Western blot protein bands for each group of mice. (b) Western blot protein band intensities were quantified and normalized to GAPDH band intensities. (c) Magnitude change of oxy-, deoxy-, total hemoglobin, and percent oxygen saturation with an inhaled carbogen (95% $O_2$ +5% $CO_2$) challenge.

ctHHb rose with a hypercapnia challenge in the 3xTg-AD mice at 20 months. Vascular reactivity to hypercapnia challenge was significantly diminished in ctO$_2$Hb, ctHHb, and tissue oxygen saturation measurements in 3xTg-AD mice at 20 months compared to controls. No significant difference in Total Hb rise was seen between 3xTg-AD and control mice at 20 months.

## 4 Discussion

This multimodal imaging study is the first to describe the amyloid-$\beta$-dependent time course and extent of hemodynamic and vascular impairment in AD compared to normal aging in a 3xTg-AD mouse model. SFDI results showed reduced brain perfusion and oxygenation in the 3xTg-AD mice starting at eight months. Both controls and 3xTg-AD mice showed significant drops in Total Hb and ctO$_2$Hb at 20 months, but 3xTg-AD mice had 30% lower Total Hb and 8% lower tissue oxygen saturation than controls. This mirrors findings of decreased cerebral blood flow in normal human aging,[26,27] the severity of which increases in mild cognitive impairment and AD.[28] 3xTg-AD mice exhibited a 29% decrease in vessel volume fraction compared to controls, despite upregulation of eNOS in both 3xTg-AD and control mice. Thus, eNOS inefficiency at producing the vasodilatory molecule NO in aged endothelial cells[29] may be further exacerbated by amyloid-$\beta$[30,31] in the 3xTg-AD mice. Similarly, amyloid-$\beta$ binds VEGF and limits its efficacy in inducing angiogenesis,[32] showcased in the 3xTg-AD mice by the 35% decrease in vessel density compared to controls. These data suggest that both reductions in vascular tone and density contribute to the brain hypoxia seen in AD.

Hypercapnia challenges also revealed a dynamic contrast between the 3xTg-AD and control mice at 20 months of age. In controls, we saw an expected robust increase in ctO$_2$Hb and a symmetric drop in ctHHb. However, in 3xTg-AD mice, the same challenge produced a significantly lower change for both ctO$_2$Hb and ctHHb. This could reflect an oxygen-starved state in the 20-month 3xTg-AD mice. Interestingly, nNOS

protein, which is largely responsible for vasodilation in response to hypercapnia,[33] did not change with age or between AD and normal mice. Hypercapnia is known to increase heart rate and ventilation in addition to vessel dilation.[34] Thus, without control of the former two variables, interpretation of these results is limited.

Multimodality information allowed us to calculate the mean apparent hematocrit for the 20-month control and 3xTg-AD mice to be 0.16 and 0.17, respectively. Normal hematocrit for young C57 BL6 mice is $0.44 \pm 0.004$.[23] While it is possible that the true hematocrit is as low as the calculated apparent hematocrit, the different tissue depths interrogated by SFDI ($\sim$2 to 4 mm) and dOCT ($\sim$200 $\mu$m) have different vessel volume fractions. For example, SFDI probes relatively deep cortical and subcortical structures. If the observed vessel fraction is less than that of the regions measured by dOCT, the apparent hematocrit would increase. Nevertheless, dOCT images suggest that SFDI-measured alterations in bulk tissue hemodynamic properties are due to underlying changes in microvascular structure rather than differences in erythrocyte volume fraction between AD and control mice.

Reduced scattering coefficients were significantly elevated in the 20-month 3xTg-AD mice compared to controls, and $\mu_s'$ increased with age in both 3xTg-AD and control mice. Tissue scattering parameters are measured in SFDI (instead of assumed in continuous wave spectroscopy), yielding more accurate absorption values in addition to general structural contrast. For example, cell or organelle swelling from cerebral edema,[35] vasodilation from cortical activation,[36] *ex vivo* human AD brain tissue,[37] and cell death *in vitro*[38] and *ex vivo*[39] all alter light scattering. We found the measured skull thickness correlates to the increase in scattering with age. Better modeling of light through layered tissue and further study of a mouse model that mimics the cellular pathology seen in human AD[40] will need to be done to make the scattering signal an informative biomarker of AD.

In summary, we have utilized complementary *in vivo* optical imaging methods, SFDI and dOCT, combined with conventional histological and protein assays, in a longitudinal mouse model study examining the appearance and progression of AD. Our results suggest that amyloid-$\beta$ may contribute to ischemia/hypoxia in the brain of 3xTg-AD mice by reducing both vessel density and volume *in vivo*, despite upregulated VEGF and eNOS protein. This work links *in vivo* hemodynamic measurements to molecular biomarkers in a preclinical model and suggests potential approaches for utilizing clinical near-infrared spectroscopy/diffuse optical imaging for characterizing AD vascular pathology and response to therapy in patients.

## References

1. C. Iadecola, "Neurovascular regulation in the normal brain and in Alzheimer's disease," *Nat. Rev. Neurosci.* **5**(5), 347–360 (2004).
2. H. W. Querfurth and F. M. LaFerla, "Alzheimer's disease," *N. Engl. J. Med.* **362**(4), 329–344 (2010).
3. E. Vicenzini et al., "Cerebrovascular reactivity in degenerative and vascular dementia: a transcranial Doppler study," *Eur. Neurol.* **58**(2), 84–89 (2007).
4. M. Silvestrini et al., "Cerebrovascular reactivity and cognitive decline in patients with Alzheimer disease," *Stroke* **37**(4), 1010–1015 (2006).
5. A. Stefani et al., "CSF biomarkers, impairment of cerebral hemodynamics and degree of cognitive decline in Alzheimer's and mixed dementia," *J. Neurol. Sci.* **283**(1–2), 109–115 (2009).
6. U. S. Yezhuvath et al., "Forebrain-dominant deficit in cerebrovascular reactivity in Alzheimer's disease," *Neurobiol. Aging* **33**(1), 75–82 (2012).
7. A. Kassner et al., "Blood-oxygen level dependent MRI measures of cerebrovascular reactivity using a controlled respiratory challenge: reproducibility and gender differences," *J. Magn. Reson. Imaging* **31**(2), 298–304 (2010).
8. G. Stoppe et al., "Cerebrovascular reactivity to acetazolamide in (senile) dementia of Alzheimer's type: relationship to disease severity," *Dementia* **6**(2), 73–82 (1995).
9. L. Pavics et al., "rCBF SPECT and the acetazolamide test in the evaluation of dementia," *Nucl. Med. Rev. Cent. East. Eur.* **1**(1), 13–19 (1998).
10. H. K. Shin et al., "Age-dependent cerebrovascular dysfunction in a transgenic mouse model of cerebral amyloid angiopathy," *Brain* **130**(9), 2310–2319 (2007).
11. S. Takeda et al., "Angiotensin receptor blocker prevented beta-amyloid-induced cognitive impairment associated with recovery of neurovascular coupling," *Hypertension* **54**(6), 1345–1352 (2009).
12. D. Puzzo et al., "Phosphodiesterase 5 inhibition improves synaptic function, memory, and amyloid-beta load in an Alzheimer's disease mouse model," *J. Neurosci.* **29**(25), 8075–8086 (2009).
13. X. Sun et al., "Hypoxia facilitates Alzheimer's disease pathogenesis by up-regulating BACE1 gene expression," *Proc. Natl. Acad. Sci. U S A* **103**(49), 18727–12732 (2006).
14. X. Zhang et al., "Hypoxia-inducible factor 1alpha (HIF-1alpha)-mediated hypoxia increases BACE1 expression and beta-amyloid generation," *J. Biol. Chem.* **282**(15), 10873–10880 (2007).
15. T. D. O'Sullivan et al., "Diffuse optical imaging using spatially and temporally modulated light," *J. Biomed. Opt.* **17**(7), 071311 (2012).
16. A. J. Lin et al., "Spatial frequency domain imaging of intrinsic optical property contrast in a mouse model of Alzheimer's disease," *Ann. Biomed. Eng.* **39**(4), 1349–1357 (2011).
17. D. J. Cuccia et al., "Modulated imaging: quantitative analysis and tomography of turbid media in the spatial-frequency domain," *Opt. Lett.* **30**(11), 1354–1356 (2005).
18. R. D. Frostig, *In Vivo Optical Imaging of Brain Function*, 2nd ed., CRC Press, Boca Raton (2009).
19. A. Lajtha, G. E. Gibson, and G. A. Dienel, *Handbook of Neurochemistry and Molecular Neurobiology. Brain Energetics, Integration of Molecular and Cellular Processes*, 3rd ed., Springer, New York (2007).
20. C. Ayata et al., "Laser speckle flowmetry for the study of cerebrovascular physiology in normal and ischemic mouse cortex," *J. Cereb. Blood Flow Metab.* **24**(7), 744–755 (2004).
21. D. J. Cuccia et al., "Quantitation and mapping of tissue optical properties using modulated imaging," *J. Biomed. Opt.* **14**(2), 024012 (2009).
22. G. Liu et al., "High-resolution imaging of microvasculature in human skin in-vivo with optical coherence tomography," *Opt. Express* **20**, 7694–7705 (2012).
23. E. S. Russell, E. F. Neufeld, and C. T. Higgins, "Comparison of normal blood picture of young adults from 18 inbred strains of mice," *Proc. Soc. Exp. Biol. Med.* **78**(3), 761–766 (1951).
24. W. S. Rasband, *ImageJ*, U.S. National Institutes of Health, Bethesda, Maryland (1997-2012).
25. S. M. White, S. C. George, and B. Choi, "Automated computation of functional vascular density using laser speckle imaging in a rodent window chamber model," *Microvasc. Res.* **82**(1), 92–95.
26. Y. Liu et al., "Arterial spin labeling MRI study of age and gender effects on brain perfusion hemodynamics," *Magn. Reson. Med.* **68**(3), 912–922 (2012).
27. K. L. Leenders et al., "Cerebral blood flow, blood volume and oxygen utilization. Normal values and effect of age," *Brain* **113**(1), 27–47 (1990).
28. N. Schuff and X. P. Zhu, "Imaging of mild cognitive impairment and early dementia," *Br. J. Radiol.* **80**(Spec No 2), S109–S114 (2007).
29. Y. M. Yang et al., "eNOS uncoupling and endothelial dysfunction in aged vessels," *Am. J. Physiol. Heart Circ. Physiol.* **297**(5), H1829–H1836 (2009).
30. M. T. Gentile et al., "Mechanisms of soluble beta-amyloid impairment of endothelial function," *J. Biol. Chem.* **279**(46), 48135–48142 (2004).
31. Z. Khalil et al., "Mechanisms of peripheral microvascular dysfunction in transgenic mice overexpressing the Alzheimer's disease amyloid Abeta protein," *J. Alzheimers Dis.* **4**(6), 467–478 (2002).
32. S. P. Yang et al., "Co-accumulation of vascular endothelial growth factor with beta-amyloid in the brain of patients with Alzheimer's disease," *Neurobiol. Aging* **25**(3), 283–290 (2004).
33. J. E. Brian, Jr., "Carbon dioxide and the cerebral circulation," *Anesthesiology* **88**(5), 1365–1386 (1998).
34. R. S. Kronenberg and C. W. Drage, "Attenuation of the ventilatory and heart rate responses to hypoxia and hypercapnia with aging in normal men," *J. Clin. Invest.* **52**(8), 1812–1819 (1973).
35. A. S. Gill et al., "Early optical detection of cerebral edema in vivo," *J. Neurosurg.* **114**(2), 470–477 (2011).
36. K. Tanner et al., "Spectrally resolved neurophotonics: a case report of hemodynamics and vascular components in the mammalian brain," *J. Biomed. Opt.* **10**(6), 064009 (2005).
37. E. B. Hanlon et al., "Scattering differentiates Alzheimer disease in vitro," *Opt. Lett.* **33**(6), 624–626 (2008).
38. C. S. Mulvey, C. A. Sherwood, and I. J. Bigio, "Wavelength-dependent backscattering measurements for quantitative real-time monitoring of apoptosis in living cells," *J. Biomed. Opt.* **14**(6), 064013 (2009).
39. P. B. Garcia-Allende et al., "Automated identification of tumor microscopic morphology based on macroscopically measured scatter signatures," *J. Biomed. Opt.* **14**(3), 034034 (2009).
40. T. R. Yamasaki et al., "Neural stem cells improve memory in an inducible mouse model of neuronal loss," *J. Neurosci.* **27**(44), 11925–11933 (2007).

**Alexander J. Lin** is an MD/PhD student in the Medical Scientist Training Program at the University of California, Irvine (UCI). He received his PhD from the Department of Biomedical Engineering at UCI in 2013, working in the lab of Dr. Bruce Tromberg at the Beckman Laser Institute (BLI). He is currently completing medical school at UCI.

**Gangjun Liu** is an assistant professor at Casey Eye Institute, Oregon Health and Science University. Before that, he was with BLI, University of California. His research interest is optical coherence tomography, especially functional optical coherence tomography.

**Nicholas A. Castello** is a postdoctoral fellow at the Gladstone Institutes in San Francisco, California, in the laboratory of Dr. Katerina Akassoglou. His research is focused on the role of blood-brain barrier disruption in neurological disease and injury. In particular, his work investigates the impact that extravasated blood proteins have on inflammation and neuronal function. He completed his PhD in neurobiology and behavior at UCI in 2013.

**James J. Yeh** worked as an undergraduate researcher at UCI's Epilepsy Research Center and as a junior investigator at UCI's Beckman Laser Center.

**Rombod Rahimian** is an assistant specialist at BLI of UCI. He holds a BS in biological sciences and BA in art history from UCI and is currently completing an MPH with a concentration in global health from the University of Arizona.

**Grace Lee** is an undergraduate biology student at UCI. She plans on going to a graduate school after the completion of her bachelor's degree in biological sciences at UCI. Her ultimate goal is to become a physician assistant.

**Victoria Tsay** is a senior in the UCLA Bioengineering undergraduate program. She plans to pursue a master's degree in bioengineering and eventually a career in biotechnology. Her research interests include combinational drug therapy and cardiovascular morphology in zebrafish.

**Anthony J. Durkin** is an associate professor at BLI of UCI. His research is focused on the development and application of optical spectroscopic and quantitative wide-field imaging techniques to characterize superficial tissues *in vivo*. He is codirector of the Wide-field Functional Imaging Program at BLI. He holds a PhD in biomedical engineering from the University of Texas at Austin with emphasis on biomedical optics and spectroscopy.

**Bernard Choi** is an associate professor of biomedical engineering and surgery at UCI, with a primary appointment at BLI. He received a BS from Northwestern University and PhD degree from the University of Texas at Austin, all in biomedical engineering. His current research is in the field of vascular biophotonics, with current emphases in optical hemodynamic monitoring, microvascular dynamics of tissue in normal and proliferative states, and optical clearing.

**Frank M. LaFerla** is the Hana and Francisco J. Ayala dean of biological sciences. He is a chancellor's professor in the Department of Neurobiology and Behavior, where he also served as the chair from 2010 to 2013, and is the director of UCI MIND. His research focuses on understanding the pathogenesis of Alzheimer disease, the most common form of dementia.

**Zhongping Chen** received his PhD degree in applied physics from Cornell University in 1992. He joined BLI of UCI in 1995 and is currently a full professor of biomedical engineering at UCI. His research experience and interests are in the areas of biomedical optics, photonic materials and devices, biomaterials, and biosensors.

**Kim N. Green** is currently an assistant professor in the Department of Neurobiology and Behavior at UCI, and a member of the Institute for Memory Impairments and Neurological Disorders. He received his PhD from the University of Leeds in 2003 and studies neurodegenerative diseases, particularly Alzheimer's disease.

**Bruce J. Tromberg** is the director of the BLI at UCI and principal investigator of the Laser Microbeam and Medical Program, an NIH P41 National Biomedical Technology Center in the BLI. He is a professor with joint appointments in the Departments of Biomedical Engineering and Surgery and has been a member of the UCI faculty since 1990.